Effects of Induction Hardening and Prior Cold Work on a Microalloyed Medium Carbon Steel*

J.L. Cunningham, D.J. Medlin, and G. Krauss

(Submitted 21 December 1998; in revised form 15 March 1999)

The torsional strength and microstructural response to induction hardening of a 10V45 steel with prior cold work was evaluated. The vanadium-microalloyed 1045 (10V45) steel was characterized in three conditions: as-hot-rolled, 18% cold-reduced, and 29% cold-reduced. Two of these evaluations, 10V45 as-hot-rolled and 10V45-18%, were subjected to stationary and progressive induction hardening to three nominal case depths: 2, 4, and 6 mm. All specimens were subsequently furnace tempered at 190 °C for 1 h. The martensitic case microstructures contained residual lamellar carbides due to incomplete dissolution of the pearlitic carbides in the prior microstructure. Torsional overload strength, as measured by maximum torque capacity, is greatly increased by increasing case depth, and to a lesser extent by increasing prior cold work level. Maximum torque capacity ranges from 2520 to 3170 N · m, depending upon induction hardening processing. Changing induction hardening processing from stationary (single-shot) to progressive (scan) had little effect on torque capacity.

Keywords induction hardening, medium carbon steel, torsional strength

1. Introduction

Monotonic torsional strength of induction hardened shafts is greatly influenced by the depth and hardness of the case, as well as the hardness of the core, as was shown by Ochi and Koyasu (Ref 1). Figure 1 shows that as case depth and carbon content increase, torsional strength increases. Likewise, as hardness increases, whether in the core or in the case, torsional strength increases, as shown in Fig. 2. This effect is also shown for varying case depths.

Cost reduction measures in manufacturing industries, particularly within the automotive industry, have led to reduced material consumption and elimination of processing steps where possible. With the addition of small amounts of vanadium, niobium, and/or titanium, microalloyed steels provide high strength with a minimum of heat treatment processing (Ref 2). Material costs are reduced due to the lowering of alloy additions, and processing costs are reduced due to the elimination of heat treating steps.

Microalloyed, medium carbon steels gain their strength from the precipitation of carbonitrides during cooling after austenitization. Strengths typical of highly tempered martensitic steels are obtained by pearlite formation and precipitation strengthening. Toughness is low, but can be increased by grain size refinement or by limiting alloy carbon content (Ref 2-5). Because the strengthening effects are exhibited in the direct-cooled, ferritic-pearlitic microstructures, heat treatment subsequent to rolling or forging is not necessary (Ref 2).

*This paper was originally presented at the 17th ASM Heat Treating Society Conference, which included the 1st International Induction Heat Treating Symposium, 1997.

J.L. Cunningham, American Axle and Manufacturing, Rochester Hills, MI; **D.J. Medlin**, Timken Co., Canton, OH; and **G. Krauss,** Colorado School of Mines, Golden, CO. Contact e-mail: gkrauss@mines.edu.

High core strength provides a means of increasing performance of induction hardened shafts, and microalloying is one method used to increase the core strength. Also, because strength increases directly with the amount of cold work (Ref 6), it may be possible to use cold reduction concurrently with microalloying to provide a core with high strength.

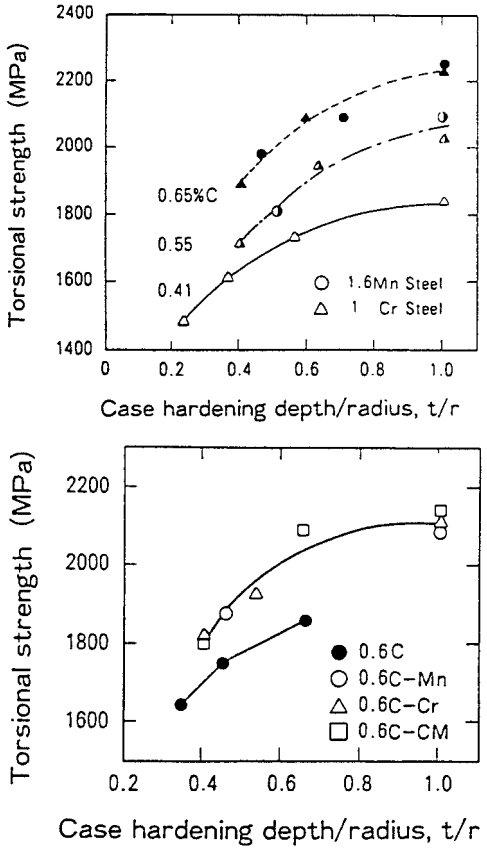

Fig. 1 Torsional strength as a function of case depth for various grades of steel. Source: Ref 1

In the process of induction hardening there are two concerns regarding phase transformation: dissolution and precipitation of second-phase particles and austenitization mechanism at fast heating times. Both issues are well understood from an equilibrium perspective but less understood for nonequilibrium conditions. Because induction hardening is not a slow heating or slow cooling process, the solubility of not only the microalloy carbonitrides, but also the pearlitic carbides, is greatly dependent on heating time, not just temperature. Of major concern is the complete dissolution of the microalloying elements and other carbonitride formers during induction heating.

The purpose of this paper is to examine benefits associated with the use of induction hardened microalloyed steel, with and without cold work. Some information regarding carbide retention during induction hardening is also presented.

2. Experimental Procedure

Materials. A commercially produced 10V45 (SAE 1045, modified with vanadium) was provided by Inland Steel in 33 mm round bars. Table 1 gives the chemical composition of the steel. The 10V45 was cold drawn to two levels of cold work, 18 and 29%, resulting in final diameters of 29.9 and 27.8 mm, respectively. These three materials are designated 10V45-0, 10V45-18, and 10V45-29 for the as-hot-rolled, 18% cold-drawn, and 29% cold-drawn bars, respectively.

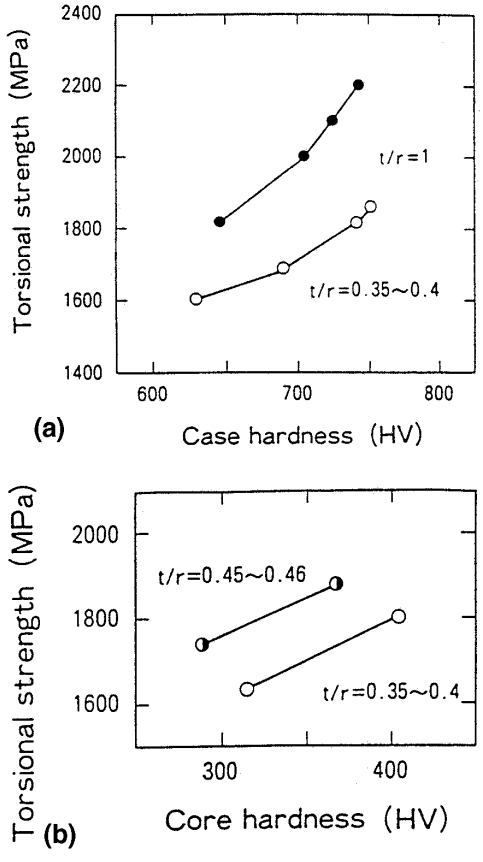

Fig. 2 Torsional strength as a function of (a) case hardness and (b) core hardness for various case depths, where t is case depth and r is bar radius. Source: (Ref 1)

Hardness Profiles. Hardness of all material conditions was measured with both the Vickers and Rockwell C scales. At least three sections of each material, approximately 13 mm in height, were ground to a 6 μm diamond finish. Vickers microhardness profiles along the radii of the sections were measured on a LECO M-400A (St. Joseph, MI) hardness tester with a 1000 g load and a 55× objective lens. Point measurements of Rockwell C hardness were measured on a LECO R-600 hardness tester with a 1 kg load. Vickers hardness data were converted to Rockwell C scale using standardized conversion tables (Ref 7).

Metallography. Specimens of all material conditions were polished to a 1 μm diamond finish and observed on an Ausjena Neophot 21 light metallograph. Both longitudinal and transverse oriented specimens were observed. Ferrite volume fraction, ferrite grain size, and decarburization depth were measured by standard techniques (Ref 8-10). All specimens were etched in a 2% nital solution.

Tensile Testing. Tensile tests were conducted on an Instron 1125 screw-type mechanical testing machine (Instron Corp., Canton, MA), with analog-to-digital data acquisition. Round tensile specimens were machined from the center of the as-hot-rolled and cold-drawn bars. Gage length was 25.4 mm (1.00 in.). Tests were run in triplicate and at room temperature with a crosshead speed of 1.27 mm/min (0.05 in./min).

Table 1 Composition of 10V45 steel

Element	Composition, wt%
C	0.440
Mn	0.870
P	0.016
S	0.025
Si	0.260
Ni	0.050
Mo	0.020
Cr	0.018
V	0.120
Al	0.023
Cu	0.080
N	0.013
O	0.0018

Table 2 Full factorial experimental test matrix for the induction hardened conditions

Run No.	Material	Method	Case depth, mm
1	10V45-0	Scan	2.0
2	10V45-0	Scan	4.0
3	10V45-0	Scan	6.0
4	10V45-0	Single shot	2.0
5	10V45-0	Single shot	4.0
6	10V45-0	Single shot	6.0
7	10V45-18	Scan	2.0
8	10V45-18	Scan	4.0
9	10V45-18	Scan	6.0
10	10V45-18	Single shot	2.0
11	10V45-18	Single shot	4.0
12	10V45-18	Single shot	6.0

Electron Microscopy. Electron microscopy was conducted on a JEOL JX-840 scanning electron microscope (Peabody, MA). Metallographic specimens were viewed with a 1 μm diamond polish and a 15:6:1 H_2O: dodecylbenzesulfonic acid, sodium salt: picric acid etching solution, heated to approximately 80 °C.

Machining of Test Shafts. One hundred test shafts were made from each of the three initial material conditions: 10V45-0, 10V45-18, and 10V45-29. The shafts were approximately 330 mm (13 in.) in length and 25 mm (1 in.) in diameter. All case depths were measured at the smallest diameter on the shaft (henceforth referred to as the reference region).

Induction Hardening. Two material conditions were selected, 10V45-0 and 10V45-18, to undergo induction hardening heat treatment. Induction hardening of the test shafts was conducted with both stationary (single-shot) and progressive (scan) methods.

An experimental test matrix was defined, which tested the effects of material, hardening method, and case depth on torsional overload strength. Table 2 shows the test matrix. The matrix is full factorial, testing the two material conditions, the two hardening methods, and three nominal case depths of 2, 4, and 6 mm. Torsional overload strength is the response variable.

Table 3 gives the equipment setup for the differing hardened conditions. All conditions were run on a 400 kW, 3/10 kHz invertor. It was necessary to adjust the invertor for the 6 mm cases by adding capacitance. Peak temperatures were not measured due to equipment limitations. All shafts were quenched to 24 °C (76 °F) with a 2% concentration of Houghton Aqua Quench 251 polymer quenching media. Quenchant flow rate was 7.6 L/s at 276 MPa and 5.1 L/s at 207 MPa (120 gpm at 40 psi and 80 gpm at 30 psi) for the single-shot and scanned shafts, respectively. To confirm correct setup, case depths were verified with a Brinell glass at the reference region of the shaft (undercut). All induction hardened shafts were subjected to the same furnace temper treatment: 190 °C (375 °F) for 1 h (Ref 11).

Torsion Testing. Torsional overload strength was chosen as the response variable to the experimental induction hardening matrix, given in Table 2. Two shafts of each hardened condition (24 total) were tested. Twist rate was set at 10 to 20° per minute, and shafts were tested through a maximum of 20° of twist to map yielding and maximum torque applied. Once maximum torque was reached, and torque began to drop, the test was suspended. Shafts were fit into the test fixture to full spline engagement. Maximum torque is the specific variable measured in response to the varied induction hardened conditions.

Table 3 Equipment setup for the six induction hardening conditions used in this study

Scan rate	Case depth, mm	Dwell time, s	Power, kW	Frequency, kHz
Single shot	2	4.0	200 (50%)	8.0-9.0
	4	4.8	200 (50%)	8.0-9.0
	6	4.8	224 (56%)	7.5-8.6
0.8 in./s	2	0.1	84 (21%)	8.2
	4	0.1	110 (27.5%)	9.0
	6	0.1	136 (34%)	5.5

3. Prehardening Results

Microstructure. The as-hot-rolled microstructure of the 10V45-0 is ferritic-pearlitic, with a ferrite volume fraction of 34.8%, a ferrite grain size of 5.3 μm, and a pearlite interlamellar spacing of 0.34 μm. The 18% cold-drawn microstructure of the 10V45-18 exhibits the development of cold-worked microstructure and a decrease in ferrite grain size to 5.0 μm. The 29% cold-drawn microstructure of the 10V45-29 shows the increased effect of cold work. The ferrite grain size decreased to 4.7 μm. The decrease in grain size with increased cold work is not attributed to a grain refinement phenomena but to the simple elongation of the grains with deformation. Table 4 summarizes the metallographic data.

Hardness. The initial hardness profiles through the as-received bars were flat. With increasing cold work, 10V45 steel shows an increase in average hardness from 23 HRC for the 10V45-0 steel, to 30 HRC for the 10V45-18 steel, and to 37 HRC for the 10V45-29 steel. Figure 3 gives a summary of the hardness data for these steels.

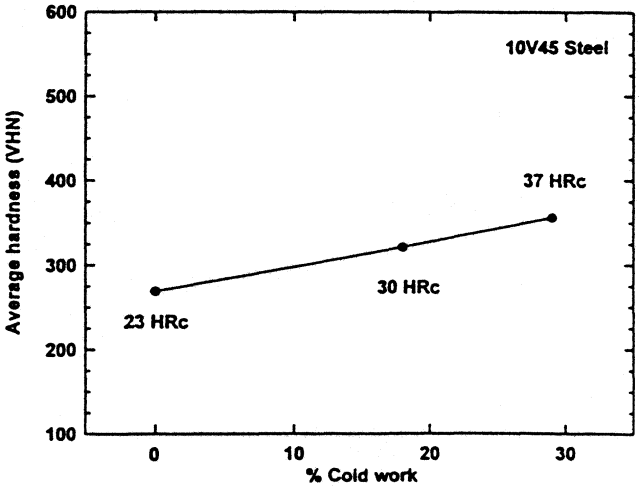

Fig. 3 Comparison of the as-received hardness for the three steels evaluated in this study

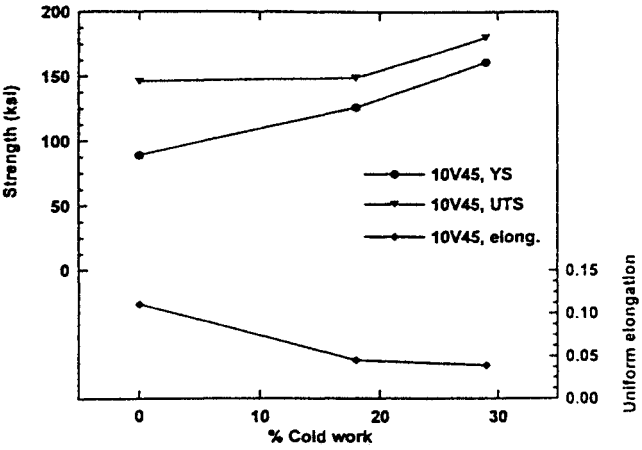

Fig. 4 Comparison of tensile properties for the three steels evaluated in this study

Strength and Ductility. With increased cold work, ductility, as exhibited by uniform elongation, was dramatically reduced, while yield strength and ultimate strength were increased. Uniform elongation decreased from 11% for the 10V45-0 steel to 3.9% for the 10V45-29 steel. Yield strength ranged from 614 MPa (89 ksi) for the as-hot rolled steel to 1111 MPa (161 ksi) for the 29% cold-drawn steel. Ultimate strength ranged from 1007 MPa (146 ksi) to 1242 MPa (180 ksi). Figure 4 and Table 5 summarize these results.

Table 4 Summary of metallographic data for 10V45 steel in the as-hot-rolled, 18% cold-drawn, and 29% cold-drawn conditions

Steel	Ferrite volume fraction, %	Ferrite grain size, μm	Pearlite interlamellar spacing, μm
10V45-0	34.8 ± 1.8	5.29 ± 0.30	0.34 ± 0.05
10V45-18	…	4.96 ± 0.38	…
10V45-29	…	4.56 ± 0.23	…

Hardness. Figures 5 and 6 show the induction hardened profiles for the 10V45-0 and 10V45-18 initial conditions, respectively, each hardened to case depths of 2, 4, and 6 mm. Maximum case hardness is typically at or above 55 HRC, consistent with 0.45% carbon martensite tempered at 195 °C for 1 h (Ref 2).

When compared to single-shot profiles, scanned profiles typically show a slightly higher average case hardness of 57 HRC and slightly shallower case penetration. Cold-worked

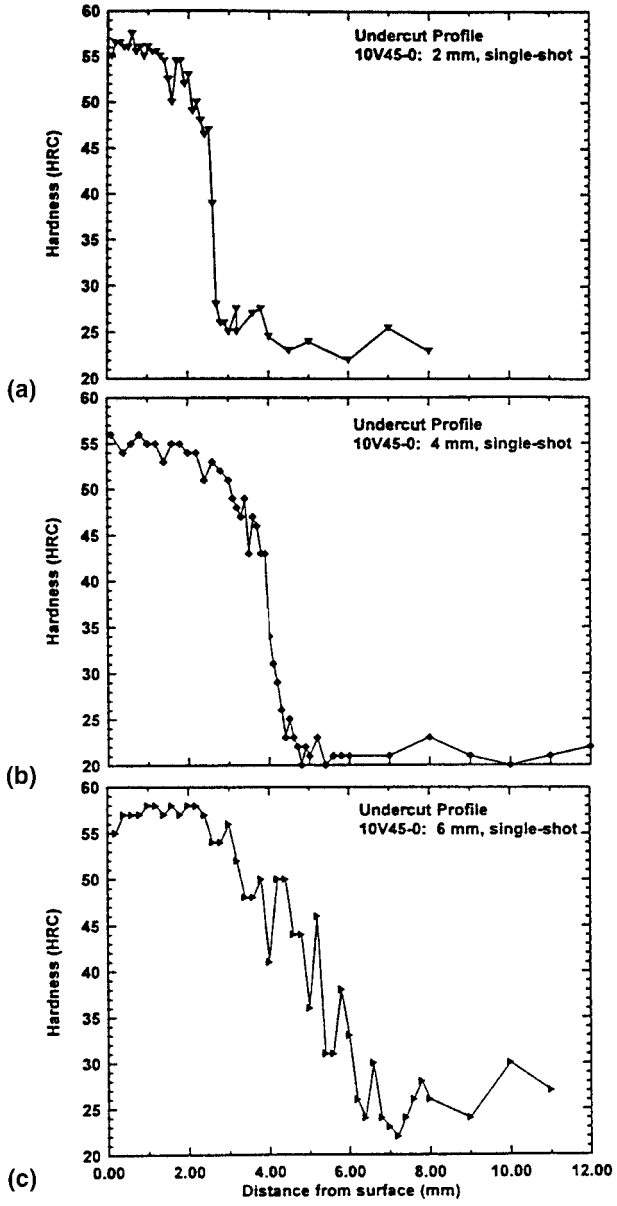

Fig. 5 Hardness profile of single-shot induction hardened 10V45-0 shafts with a case depth of (b) 4 mm

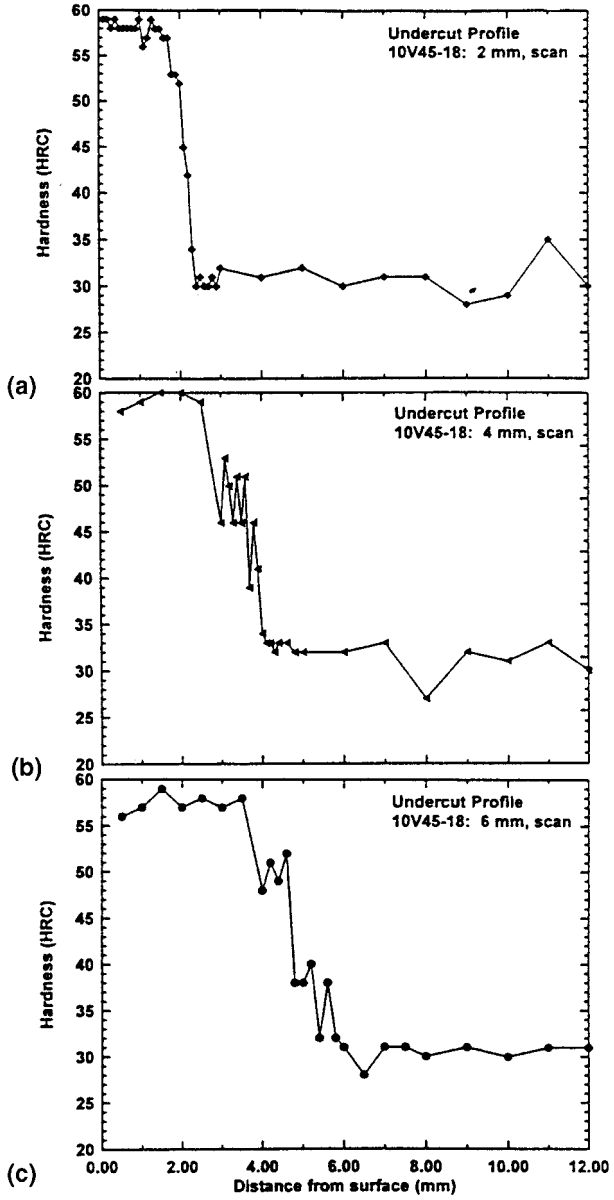

Fig. 6 Hardness profile of scan induction hardened 10V45-18 shafts with a case depth of (b) 4 mm

steel profiles, as compared to as-hot-rolled steel for the same coil type, show slight, if any, differences in peak hardness and case penetration.

Microstructure. The scan coil produced a slightly coarser martensitic microstructure than the single-shot coil. More notable is the dramatic change in microstructure caused by changing case depth. As the case depth increases, a coarser martensitic microstructure is obtained. The austenitic grain size, and therefore the martensitic laths and packet size, become larger and more visible.

Figures 7 and 8 show scanning electron micrographs of examples of the case microstructures. These micrographs not only reveal prior austenitic grain size but also the presence of lamellar carbides, revealed by a picric acid etch, in what are assumed, from hardness measurements, to be fully martensitic microstructures. These carbides closely resemble the prior pearlitic microstructure and have been termed "ghost pearlite" by Medlin et al. (Ref 12), according to industry terminology. Changes in microstructure due to coil geometry are less obvious, but changes in structure due to changes in case depth are readily observed. The ghost pearlite, present in the 2 mm cases, gives way to a more martensitic structure, which becomes nearly fully martensitic in the 6 mm cases. Likewise, prior-austenite grain size increases as case depth increases, from approximately 10 μm in the 2 mm case to approximately 30 μm in the 6 mm case. Temperatures achieved by induction hardening were not measured, but reasonable measurements of time were available. From this information time-temperature cycles to produce the various case depths by single shot and scan induction hardening were estimated and are shown schematically in Fig. 9.

Table 5 Summary of tensile properties for the three experimental steels used inthis study

Steel	Yield strength, MPa (ksi)	Ultimate strength, MPa (ksi)	Uniform elongation, %
10V45-0	614 (89)	1007 (146)	11
10V45-18	870 (126)	1029 (149)	4.5
10V45-29	1111 (161)	1242 (180)	3.9

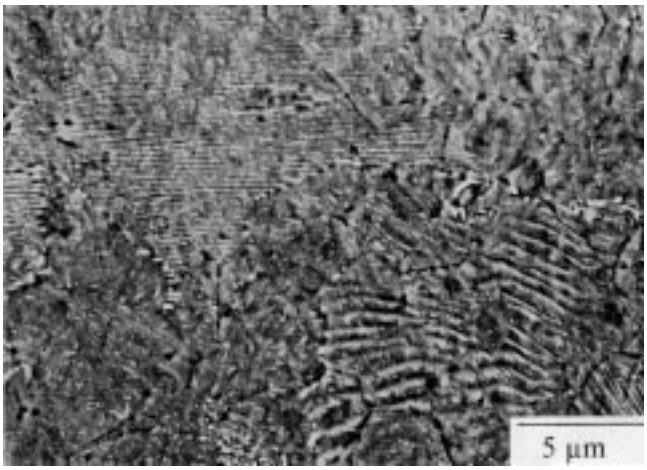

Fig. 7 Scanning electron microscopy image showing ghost pearlite in the induction hardened 2 mm case microstructure

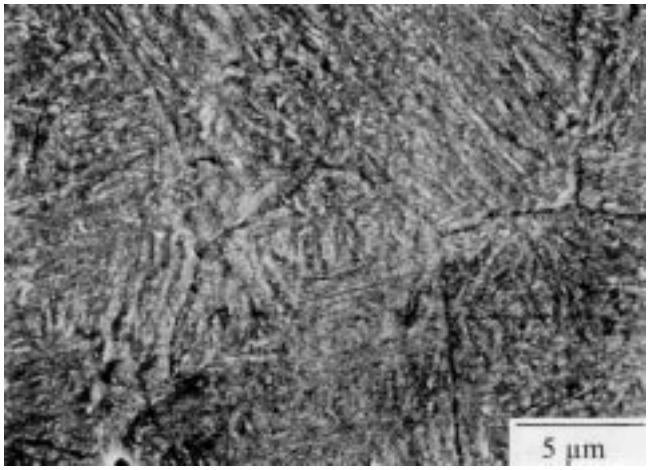

Fig. 8 Scanning electron microscopy image showing ghost pearlite in the induction hardened 6 mm case microstructure

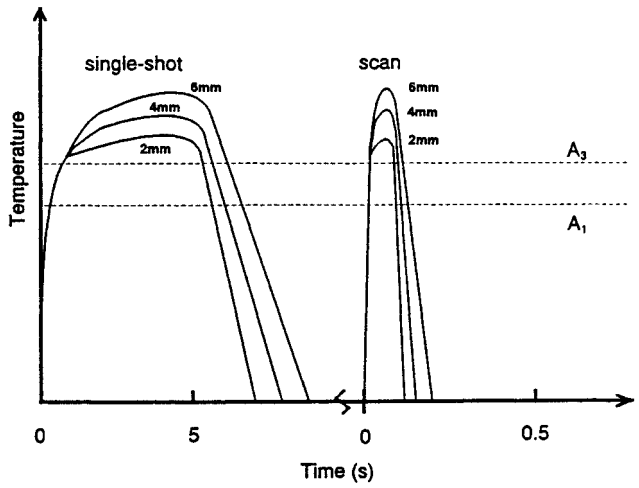

Fig. 9 Estimated time-temperature diagram showing the differences between the six induction hardened conditions

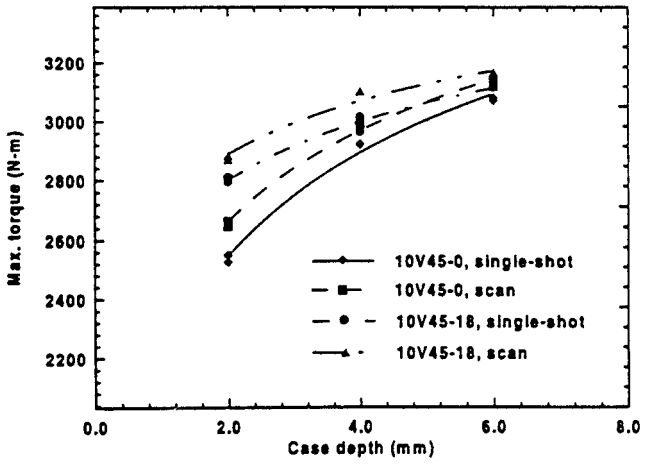

Fig. 10 Summary of the effects of case depth, cold work, and coil geometry on maximum torque capacity of induction hardened 10V45-0 and 10V45-18 shafts

Torsional Strength. Figure 10 summarizes the effect of case depth, cold work, and coil geometry on maximum torque capacity. Increased case depth has the expected effects of increasing both the yielding torque and the maximum torque of the shaft (Ref 1). A similar trend is seen with increased cold reduction. As cold work increases, maximum torque of the shaft increases, but to a smaller extent compared to the effect of case depth.

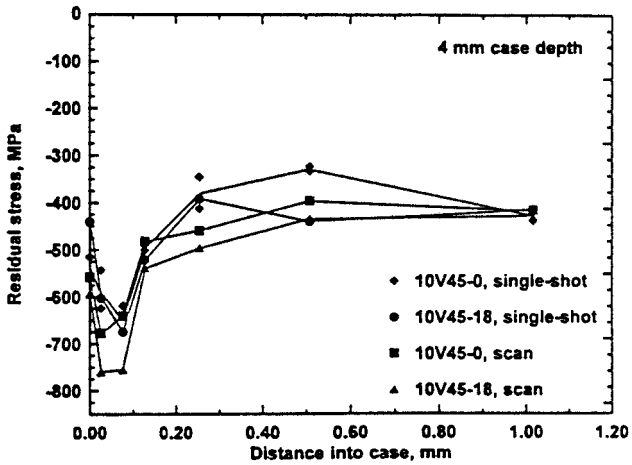

Fig. 11 Residual stress profiles of single-shot and scan induction hardened 10V45-0 and 10V45-18 shafts with 4 mm case depths

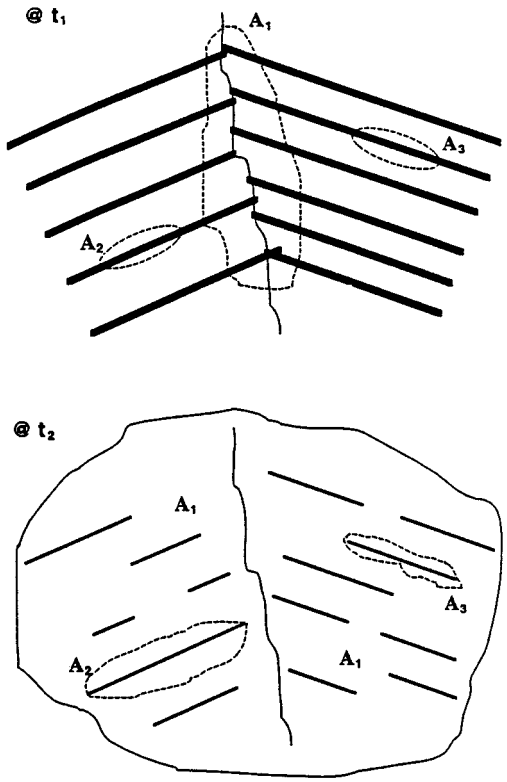

Fig. 12 Schematic representation of the austenization mechanism proposed by Speich and Szirmae for two different times, t_1 and t_2, and for three different austenite orientations, A_1, A_2, and A_3, showing interlamellar transformation. Source: Ref 23

Coil geometry is shown to have little effect on maximum torque capacity. When the induction hardening process is changed from single-shot to scan, very little, if any, difference in maximum torque is noticed. This shows that the two very different hardening processes can give similar results in torsional behavior.

At deeper case depths, the effect of cold work becomes even less significant because the mechanical effects of the deeper case begin to override the effect of prior work hardening.

Residual Stress. Figure 11 shows the residual stress profiles for the single-shot and scan induction hardening processing. The residual stress measurements were determined by standard x-ray diffraction techniques. All the profiles exhibit similar characteristics in which the maximum residual compressive stress is between 0.05 and 0.10 mm below the surface. The 10V45-18 specimen that was induction hardened by the scan method had the highest residual compressive stress of almost 780 MPa. The other specimens had maximum residual compressive stresses ranging from 620 to 680 MPa.

4. Discussion

The 10V45 steel is induction hardenable, at least from a case hardness/case depth perspective. High hardness is achieved in the case and stays acceptably high to nominal case depth. Observation of the microstructure shows a nearly martensitic structure in the case. However, a phenomenon of low pearlite dissolution, as observed in previous studies, appears, leading to a case microstructure that is not fully martensitic.

Effect of Cold Work on Induction Hardening Response. The induction hardening of the 18% cold worked 10V45 steel appeared to increase case hardness relative to that of the induction hardened as-rolled 10V45 steel, especially in the specimens induction hardened to case depths of 2 and 4 mm. This observation may be a result of the microstructural refinement produced by cold work, most quantitatively reflected in reduced ferrite grain size. The cold work may also have resulted in some fragmentation and reduction in the spacing of the pearlitic cementite lamellae. These factors, together with the increased stored strain energy of the cold worked steel, may have enhanced the formation of austenite and carbide dissolution, resulting in a higher average carbon content of the case austenite and subsequently a higher carbon martensite with an attendant higher hardness.

Effect of Induction Hardening on Case Microstructure. The short heating times involved in induction hardening tend to significantly increase the influence of variables such as maximum austenitizing temperature, prior microstructure, and cooling rate. Dissolution of second-phase particles may be more difficult, and phase transformations can occur under different conditions than typically expected. Hardenability is greatly affected. Thus, final microstructure will show differences when compared to, for example, a furnace-austenitized, quenched, and tempered microstructure of the same hardness.

The incomplete dissolution of the pearlitic cementite has been documented in this investigation. Such relatively coarse carbides may not substantially affect the overall strength of a shaft, but may influence crack initiation and propagation during fatigue or reduced fracture resistance and toughness under conditions of high load.

A limited amount of transmission electron microscopy (TEM) was performed on thin foils removed from the case regions of induction hardened specimens. Figure 12 shows schematically the model of austenite formation that was suggested by the TEM observations. Austenite nucleates either at pearlite colony interfaces or at individual cementite lamellae, consistent with earlier observations by Speich and Szirmae (Ref 12). The coarser austenite nuclei sweep across the ferrite-cementite pearlite colonies, dissolving some, but not all, of the cementite and incorporating austenite crystals that have formed locally around individual cementite lamellae.

As case depth increases, dissolution of the pearlitic cementite lamellae increases. This is assumed to be due to the increased temperature required to drive the case deeper with the same coil, regardless of single shot or scan. The temperature can be increased by either lowering the frequency or increasing the power applied to the coil, both of which occurred, according to Table 3. Increased temperature will lead to better dissolution of the pearlite (cementite lamellae) due to increased diffusion rates.

The scan induction hardening cycles in this study produced better dissolution of the pearlite than the single-shot cycles, for the same case depth. Again, this is assumed to be due to the increased temperature required to drive an equivalent case with an order-of-magnitude shorter dwell time. This is not to say that all scan hardening is better than all single-shot hardening because the two processes are not directly comparable. The magnetic physics involved (Ref 13-16) are quite different. However, a comparison of the two processes, as given in this study, dramatically shows the temperature dependence of the solution kinetics referred to earlier (Ref 17-22).

Torsional Strength Response. The torsional strength of the induction hardened shafts, represented by maximum torque capacity, has been shown to be primarily a function of case depth, with lesser effects by cold work and changes in coil geometry. The major effect of case depth was expected (Ref 1). Discussion is now limited to the slight effects of cold work, coil geometry, and microstructure.

The effect of coil geometry, or relatively low sensitivity of the induction hardened microstructure to coil geometry, cannot be construed to say that the single-shot hardening process of this study is equivalent to the scan hardening process of this study. All that can be said is that these two processes were well matched to produce shafts with equivalent strength properties and case depths.

Cold reduction has the expected effect of increasing torque capacity of induction hardened shafts. However, this effect is minor. Cold work does produce shafts that are consistently stronger than currently produced shafts, but that effect may not be separable from the effect of microalloying, which can also account for the increased performance with respect to as-produced shafts.

5. Conclusions

Mechanical and metallurgical properties of the 10V45 steel have been determined in both the as-received conditions and the induction hardened conditions. As-received conditions include as-hot-rolled, 18% cold-drawn, and 29% cold-drawn bars. Induction hardened conditions include the as-hot-rolled and 18% cold-drawn steels, with 2, 4, and 6 mm case depths, hardened by single-shot and scan induction coils. Evaluation of the properties that resulted from the induction hardening processes has led to the following conclusions:

- Prior cold work, at the levels studied, has a slight effect on hardened case microstructure, maximum case hardness, or maximum torque capacity.
- Prior cold work has the effect of producing higher case hardness when compared to as-hot-rolled microstructures hardened with the same induction hardening cycle.
- For the six given induction hardening setups, full dissolution of the pearlitic prior-microstructure does not occur, resulting in a case microstructure of high hardness, which is not fully martensitic. Arrays of lamellar carbides, described as "ghost pearlite," are present in the hardened case microstructure.
- Case microstructure, as a result of induction hardening, can be assumed to be primarily a function of austenitizing temperature at the very short heating times of induction hardening.
- Changing of induction coil geometry from single shot to scan, while not directly comparable processes, illustrated the strong temperature dependence of the mechanism of austenitization. However, changing of coil geometry does not significantly affect maximum torque capacity.
- Maximum torque capacity increases significantly with increased case depth.

Acknowledgments

This research program was performed as the M.S. thesis of Justin L. Cunningham within the Bar and Forging Steel Research Program of the Advanced Steel Processing and Products Research Center (ASPPRC), a NSF Industrial/University Cooperative Research Center at the Colorado School of Mines. The authors gratefully acknowledge the support of many individuals from the following corporations for helpful discussion, provision of steels, cold work processing, induction hardening, and testing: General Motors, Chrysler Corporation, For Motor Company, Inland Steel, Republic Engineered Steels, North Star Steel, Nelson Steel, Michigan Bar, Induction Services, Inc., The Timken Company, and Colorado School of Mines.

References

1. T. Ochi and Y. Koyasu, "Strengthening of Surface Induction Hardened Parts for Automotive Shafts Subject to Torsional Load," SAE Technical Paper Series, No. 940786, 1994
2. K. Grassl, S.W. Thompson, and G. Krauss, "New Options for Steel Selection for Automotive Applications," SAE Technical Paper Series, No. 890508, 1989
3. R.M. Landgraf and A.M. Sherman, *Micro-Alloying '75: Proceedings of the Symposium on HSLA Steels*, Vol 1-3, Oct 1975, p 498-502
4. R.S. Cline and J. McClain, *Fundamentals of Microalloying Forging Steels*, G. Krauss and S.K. Banerji, Ed., TMS/AIME, 1987, p 339-349
5. J.F. Held, *Fundamentals of Microalloying Forging Steels*, G. Krauss and S.K. Banerji, Ed., TMS/AIME, 1987, p 175-188

6. C.R. Mischke, *Standard Handbook of Machine Design*, J.E. Shigley and C.R. Mischke, Ed., McGraw-Hill, 1986, p 8.1-8.33
7. ASTM Standard E 140-88, *ASTM Annual Book of Standards*, Vol 3.01, 1991
8. ASTM Standard E 562-83, *ASTM Annual Book of Standards*, Vol 3.03, 1984, p 518-524
9. ASTM Standard E 112-84, *ASTM Annual Book of Standards*, Vol 3.03, 1984, p 120-152
10. ASTM Standard E 1077-91, *ASTM Annual Book of Standards*, Vol 3.01, 1995, p 735-744
11. D.D. Luckett, personal communication, Induction Services, Inc., Warren, Michigan, 1996
12. G.R. Speich and A. Szirmae, "Formation of Austenite from Ferrite and Ferrite-Carbide Aggregates," *Trans. AIME*, Vol 245, 1969, p 1063-1074
13. D. Giancoli, *Physics for Scientists and Engineers*, 2nd ed., Prentice Hall, Englewood Cliffs, NJ, 1988, p 628-631
14. A.F. Leatherman and D.E. Stutz, *Metal Treat.*, Vol 21 (No. 2), 1970, p 3-6, 8-12
15. N. Stevens, *ASM Handbook*, Vol 4, *Heat Treating*, 9th ed., ASM International, 1981, p 451-483
16. H.B. Osborn, Jr., "Induction Heating and Hardening," Parts A and B, ASM Home Study and Extension Courses, No. C6L11A-B, 1977
17. D.J. Medlin, G. Krauss, and S.W. Thompson, *First International Conference on Induction Hardening of Gears and Critical Components* (Indianapolis), ASM International, 1995, p 57-65
18. I.L. Yakovleva, V.M. Schastlivtsev, T.I. Tabatchikova, D.A. Mirzaev, and A.L. Osintseva, *The Physics of Metals and Metallography*, Vol 79, 1995, p 576-580
19. G.R. Speich and A. Szirmae, *Trans. AIME*, Vol 245, 1969, p 1063-1074
20. G.R. Speich, V.A. Demarest, and R.L. Miller, *Metall. Trans. A*, Vol 12, 1981, p 1419-1428
21. M. Hillert, K. Nilsson, and L.-E. Törndahl, *J. Iron Steel Inst.*, Vol 209, 1971, p 49-66
22. V.M. Schastlivtsev, I.L. Yakovleva, T.I. Tabatchikova, and D.A. Mirzaev, *J. Phys. IV*, Colloque C8, supplement *J. Phys. III*, Vol 5, December 1995, p 531-536
23. J.L. Cunningham, "Effects of Induction Hardening and Prior Cold Work on a Microalloyed Medium Carbon Steel," M.S. thesis, MT-SRC-096-024, Colorado School of Mines, Golden, Colorado, August 1996